Earth and Planetary Science Letters 388 (2014) 38–47

Contents lists available at ScienceDirect

Earth and Planetary Science Letters

www.elsevier.com/locate/epsl

How well do surface slip measurements track slip at depth in large strike-slip earthquakes? The importance of fault structural maturity in controlling on-fault slip versus off-fault surface deformation

James F. Dolan *, Ben D. Haravitch [1]

Department of Earth Sciences, University of Southern California, 3651 Trousdale Parkway, Los Angeles, CA 90089-0740, United States

ARTICLE INFO

Article history:
Received 12 July 2013
Received in revised form 21 November 2013
Accepted 22 November 2013
Available online 14 December 2013
Editor: P. Shearer

Keywords:
fault slip rates
strain localization
comparison of geologic and geodetic rate data
strain transient
structural evolution of faults
probabilistic seismic hazard assessment

ABSTRACT

Comparisons of observed surface displacements with geodetically inferred slip at depth in six large ($M_w \geqslant 7.1$) strike-slip earthquakes reveal a correlation between the structural maturity of the fault and the ratio of deep slip to surface slip that occurs on localized zones of surface rupture. Specifically, structurally immature faults ($\leqslant$25 km of total displacement) manifest only ~50–60% of total slip on narrow fault surface traces versus ~85–95% for structurally mature faults ($\geqslant$85 km total slip). The same pattern holds when structurally simple parts of a surface rupture are analyzed separately from parts that exhibit obvious structural complexity (e.g., discontinuous or multiple traces or significant dip slip). These results imply that geologic measurements of surface slip along structurally immature faults are likely to significantly underestimate the true slip at depth in large earthquakes. This observation has implications for a number of important problems, including determination of fault slip rates, which are based on surface offsets; earthquake probability assessments, which are based on geologic fault slip rates; comparisons of geologic and geodetic rate data in the search for strain transients; the structural evolution of fault zones; estimation of paleo-earthquake magnitudes based on geomorphic offsets; analyses of the relative importance of faulting vs. distributed deformation in accommodating relative plate motions in continental crust; the design and construction of infrastructure built near active faults; and possibly for the prediction of strong ground motions, which may at least partially depend on the degree of slip localization to the surface.

1. Introduction

Surface fault slip measurements are commonly used in a wide range of applications in the earth sciences, including determination of fault slip rates, comparisons of short-term geodetic with longer-term geologic rates, determination of paleo-earthquake magnitudes, and calculation of probabilistic seismic hazard. It has long been noted, however, that surface slip during earthquakes is often smaller than the slip at depth determined from geodetic and seismologic data (e.g., Thatcher and Bonilla, 1989). Recent studies show that the zone of maximum co-seismic slip in continental strike-slip earthquakes commonly occurs at about 3–6 km depth (e.g., Fialko et al., 2005; Barbot et al., 2008; Kaneko and Fialko, 2011). This difference is enhanced in models of geodetic data that incorporate a damage zone of reduced rigidity surrounding the shallow part of the fault zone (Barbot et al., 2008). If this "shallow slip deficit" is due to significant shallow off-fault deformation, as suggested by previous studies (e.g., Rockwell et al., 2002; Simons et al., 2002; Leprince et al., 2007, 2008; Ayoub et al., 2009; Shelef and Oskin, 2010), then geological surface slip measurements limited to the fault trace will systematically underestimate fault slip at depth. Consequently, any criteria based on these measurements (e.g., fault slip rates) will also be underestimated. The question arises: Is this apparent surface slip deficit the same for all faults, or does it vary as a function of measurable fault characteristics such as the structural maturity of the fault?

2. Methods

In this study, we systematically analyze the relationship between surface displacements measured at the fault trace and seismogenic slip at depth determined by static inversions of geodetic data (InSAR and GPS) for six large-magnitude (M_w 7.1–7.9) earthquakes (Table 1 and references therein). For consistency, we only consider continental earthquakes that occurred on sub-vertical

* Corresponding author. Tel.: +1 213 740 8599.
E-mail addresses: dolan@usc.edu (J.F. Dolan), ben.haravitch@gmail.com (B.D. Haravitch).
[1] Current address: Stantec Consultants, Rochester, NY, United States.

http://dx.doi.org/10.1016/j.epsl.2013.11.043

Table 1
Data sources used for estimates of slip at depth, slip at the surface, and cumulative fault displacements in the six studied earthquakes. For InSAR inversions, A = Ascending orbit, D = Descending orbit. Note that although our preferred target depth for comparison with surface slip data is 3–6 km, not all inversions have slip data available for this depth range. In such cases, we used the closest available depth range to the preferred 3–6 km depth range.

Earthquake	Inversion	Depth range	Co-seismic surface slip	Cumulative fault slip
1992 M_w 7.3 Landers	Fialko (2004); InSAR (A & D), GPS	Centered at 4 km	Liu et al. (2003)	Jachens et al. (2002)
1997 M_w 7.2 Zirkuh	Sudhaus and Jónsson (2011); InSAR (A & D, D for northern section only)	4–6 km	Berberian et al. (1999)	Walker and Jackson (2004), M. Berberian (pers. comm., 2011)
1997 M_w 7.2 Zirkuh	R. Lohman (pers. comm., 2010); InSAR (A & D)	2.66–5.33 km		
1999 M_w 7.5 Izmit	Reilinger et al. (2000); GPS	2.6–5.2 km	Duman et al. (2003)	Armijo et al. (1999)
1999 M_w 7.5 Izmit	Çakir et al. (2003); InSAR (A only)	4–8 km		
1999 M_w 7.1 Hector Mine	Jónsson et al. (2002); InSAR (A & D), SARIO, GPS	2.98–4.47 km	Treiman et al. (2002)	Jachens et al. (2002)
1999 M_w 7.1 Hector Mine	Simons et al. (2002); InSAR (A & D), GPS	Centered at 3.6 km		
2001 M_w 7.9 Kunlun	Lassere et al. (2005); InSAR (D only)	0–5 km and 5–10 km	Xu et al. (2006)	Fu and Awata (2007)
2002 M_w 7.8 Denali	Wright et al. (2004); InSAR (A & D), GPS	4–8 km	Haeussler et al. (2004a)	Reed and Lanphere (1974), Eisbacher (1976), Nockleberg et al. (1985), Lowey (1998), Miller et al. (2002), Haeussler et al. (2004a, 2004b), Benowitz et al. (2011)
2002 M_w 7.8 Denali	Elliot et al. (2007); InSAR (D only), SAR offsets, GPS	3–6 km		

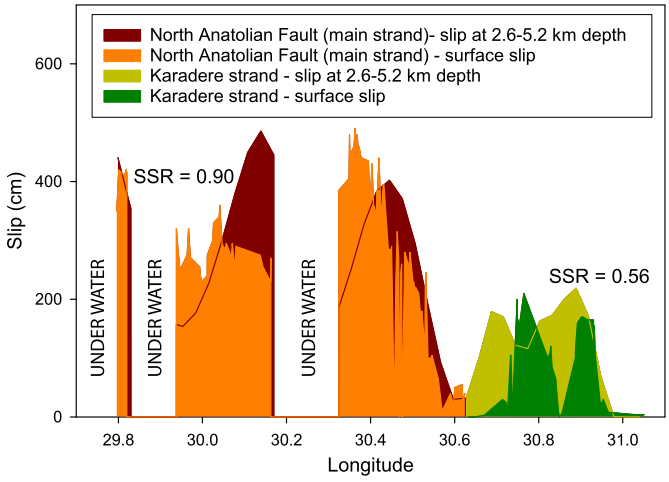

Fig. 1. Surface slip ratio (SSR) plot for the 1999 M_w 7.5 Izmit earthquake showing the area under the surface slip distribution curve (Duman et al., 2003) superimposed over the area under the curve representing slip at 2.6–5.2 km depth from Reilinger et al. (2000). SSR values represent the proportion of slip at depth transferred to the surface along a narrow localized fault rupture. This particular event is split into the two faults that ruptured because they have significantly different cumulative displacements: the main strand North Anatolian fault (orange) and the Karadere strand (green), with 85 km and 25 km of total slip, respectively (Sengor, 1979; Armijo et al., 1999). Gaps in coverage denote sections of surface rupture that are offshore in Lake Sapanca and the Gulf of Izmit. Note that it typically takes several weeks or more to complete field geological measurements of surface displacements such as those utilized in this study. Thus, these measurements will encompass both co-seismic surface slip as well as any post-seismic afterslip that might have occurred during the measurement period. Insofar as most afterslip is likely to have occurred early, the geological measurements of surface slip used in this study likely contain almost all of the total slip (co-seismic + afterslip) that has occurred along the surface trace of the fault. Similarly, the InSAR inversions used in this study as a point of comparison with the surface displacements also typically encompass time periods that would include both co-seismic slip and any early afterslip.

strike-slip faults, in which slip was predominantly horizontal. Fig. 1 shows our comparison of one specific inversion (that of Reilinger et al., 2000, for the 1999 M_w 7.5 Izmit, Turkey, earthquake) with surface slip measurements (Duman et al., 2003) to illustrate our approach. "Surface slip" is the localized slip along the fault trace, which is typically measured by geologists within a zone no more than a few meters wide; slip distributed over wider zones is commonly much more difficult to discern, and is not generally measured.

3. Observations

3.1. The "surface slip ratio"

We define the "surface slip ratio" (SSR) as the ratio of the average surface slip to the average slip at 3–6 km depth. To calculate the SSR for an earthquake we compare the area under the curve defined by surface slip as a function of distance along the fault with the area under the curve defined by the corresponding values for slip at depth. The SSR thus represents the degree to which slip at 3–6 km depth remains localized all the way to the surface for each earthquake; complete localization of slip to the surface would yield an SSR value of 1 (i.e., slip along the surface trace equals or exceeds slip at depth), whereas the absence of any localized slip along the fault trace at the surface would result in an SSR value of 0.

Although most static inversions for the same event based on geodetic data exhibit basic similarities in the slip distribution, there are differences between them. To account for this variation, wherever possible we determined SSR values for multiple inversions associated with each earthquake (Table 1). For four of the six earthquakes, we found two geodetically constrained static inversions for each earthquake; we were only able to find one suitable inversion each for the 1992 M_w 7.3 Landers and 2001 M_w 7.9 Kunlun earthquakes. We did not use slip determined from seismological data, since the variations between such inversions are commonly much larger than those between static inversions based solely on geodetic data (see examples at http://www.seismo.ethz.ch/static/srcmod/Events.html).

Fig. 2 shows the SSR values plotted as a function of cumulative fault displacement for the six earthquakes used in this study. This comparison reveals a striking correlation between the SSR values

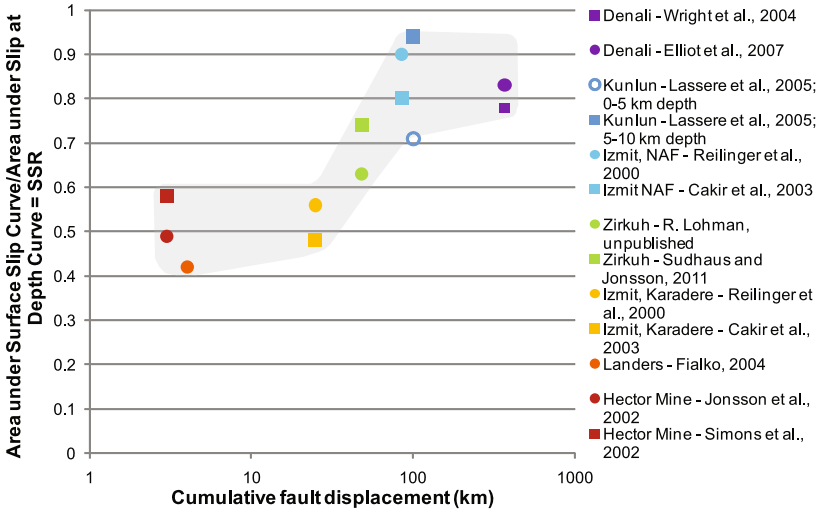

Fig. 2. Comparison of Surface Slip Ratio (SSR) with cumulative displacement of the faults that slipped during the six earthquakes that we examined. Comparisons are based on geologic surface offset data, geodetic estimations of slip at depth and geologic estimation of cumulative displacement. SSR values greater than 1 are shown as 1. Data are color-coded by fault. Different shapes represent data points calculated for the different inversions noted in Table 1. The Izmit rupture is represented here by two faults: the main strand of the NAF, with 85 km cumulative displacement, and the Karadere strand, with 25 km cumulative displacement (Sengor, 1979; Armijo et al., 1999). Note that we consider the 0–5 km data point for the 2001 Kunlun fault rupture (open circle) to be unreliable due to poor near-field coherence of the SAR data (Y. Fialko, pers. comm., 2011), but we include it for the sake of completeness.

and the structural maturity of the faults, where structural maturity is defined as the cumulative displacement of each fault (Wesnousky, 1988, and Stirling et al., 1996). Specifically, the SSR values for faults with small cumulative displacements ($\leqslant$25 km) are only 0.4–0.6, in contrast to SSR values of 0.8–0.9 for structurally mature faults with large ($\geqslant$85 km) cumulative slip. Interestingly, the one fault we examined that exhibits an intermediate cumulative displacement (the 1997 Zirkuh, Iran, earthquake [40–50 km; Walker and Jackson, 2004; M. Berberian, pers. comm., 2011]), is characterized by an intermediate SSR value of ~0.7.

It remains unclear whether there are two fundamentally different modes of behavior, separated by a narrow range of cumulative displacements somewhere between ~25 and ~85 km, or whether SSR values are more of a continuum. Analysis of more large earthquakes and ongoing studies utilizing the COSI-Corr sub-pixel image correlation technique to determine ratios of on- vs. off-fault deformation may help answer this question (e.g., Hollingsworth et al., 2012; Milliner et al., 2012).

The consistency of the correlation shown in Fig. 2 strongly suggests that the percentage of localized, on-fault surface slip that might be measured by a geologist, either after an earthquake or as part of a study of the longer-term slip rate of the fault, is not random, but rather is strongly controlled by the structural maturity of the fault. Specifically, these results indicate that, on average, surface slip measurements from structurally mature, large-cumulative-displacement faults will be more reflective of slip at depth than surface slip measurements from structurally immature, small-cumulative-slip faults. This intuitively makes sense in that structurally immature faults have many more (and larger) zones of structural complexity than mature faults (e.g., Wesnousky, 1988; Stirling et al., 1996), and such zones would be expected to exhibit a larger component of off-fault, distributed deformation, thus yielding lower SSR values (conversely, the "smoothness" of structurally mature faults allows them to host larger-magnitude earthquakes, explaining the general correspondence in Fig. 2 between SSR and M_w).

Geologists, however, will typically avoid structurally complex parts of a fault when conducting the slip-rate studies that form the basis for most probabilistic seismic hazard assessments. They focus instead on structurally simple sections of the faults, ideally those sections characterized by a single, relatively straight fault trace. Thus, since much of the near-fault distributed deformation inferred from our SSR results probably occurs in the more prevalent zones of structural complexity that characterize structurally immature faults, our SSR results may simply reflect the fact that structurally immature faults have many more such zones of structural complexity (e.g., Wesnousky, 1988; Stirling et al., 1996).

The key issue is whether the percentage of on-fault versus off-fault surface deformation is the same for the structurally simple parts of all faults. Alternatively, does the structural maturity of the fault affect the amount of off-fault distributed deformation at the surface even along the structurally simple sections of faults? In other words, do surface displacements along the structurally simple sections of ruptures on structurally immature faults systematically under-represent slip at depth to a greater degree than similar sections of surface rupture on structurally mature faults?

3.2. The "local surface slip ratio"

To find out, we examined the detailed relationship between slip at all measured points along the surface trace and the average slip at 3–6 km depth beneath that point determined from the geodetic inversions. The resulting ratio, which we refer to as the Local Surface Slip Ratio (LSSR), is similar to the SSR values described above, except that it reflects a site-specific comparison, rather than an average over the entire rupture plane. As with the SSR, an LSSR value of 1 reflects complete localization of slip from depth to the surface, whereas an LSSR value of zero reflects a complete absence of localized fault slip at the surface.

We used published maps of the surface ruptures (Berberian et al., 1999; Treiman et al., 2002; Duman et al., 2003; Haeussler et al., 2004a, 2004b; Liu et al., 2003; Xu et al., 2006) in the six studied earthquakes to distinguish between sections of relative structural complexity (steps, gaps, multiple or discontinuous fault strands, or significant non-horizontal slip), and sections having a single continuous, structurally and kinematically simple fault trace.

Despite variations amongst the different inversions, and the fact that the inversions smooth data over a multiple-kilometer scale (thus smearing out correlations with the surface measurements[2]),

[2] Most of the published inversions used in our comparative analysis do not include formal error estimates on slip measurements. Moreover, differences between

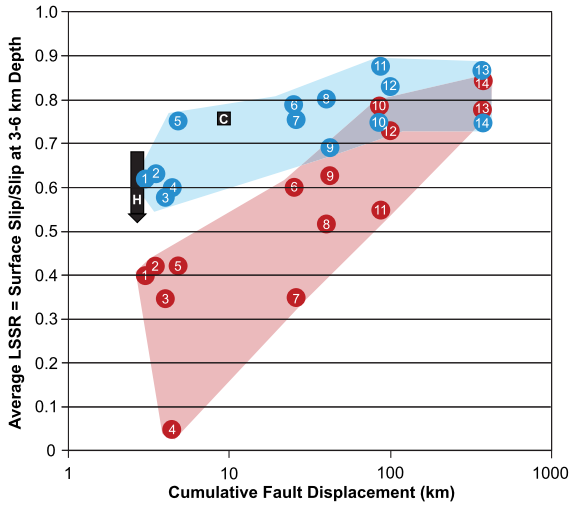

Fig. 3. Comparison of average of all Local Surface Slip Ratio (LSSR) values from each earthquake for structurally simple (blue circles) and structurally complex (red circles) sections of the faults that ruptured during the six earthquakes we examined, plotted against cumulative displacement for the faults that ruptured in these events. LSSR values greater than 1 are shown as 1. Numbers denote different pairs of static inversion-surface slip comparisons for the six different earthquakes: 1: 1999 Hector Mine, Jónsson et al. (2002); Treiman et al. (2002); 2: 1999 Hector Mine, Simons et al. (2002); Treiman et al. (2002); 3: 1992 Landers (Camp Rock/Emerson faults only), Fialko (2004); Liu et al. (2003); 4: 1992 Landers (Homestead Valley fault), Fialko (2004); Liu et al. (2003); 5: 1992 Landers (Johnson Valley fault); Fialko (2004); Liu et al. (2003); 6: 1999 Izmit (Karadere strand), Çakir et al. (2003); Duman et al. (2003); 7: 1999 Izmit (Karadere strand), Çakir et al. (2003); Duman et al. (2003); 8: 1997 Zirkuh, R. Lohman (pers. comm., 2010); Berberian et al. (1999); 9: 1997 Zirkuh, Sudhaus and Jónsson (2011); Berberian et al. (1999); 10: 1999 Izmit (main strand), Çakir et al. (2003); Duman et al. (2003); 11: 1999 Izmit (main strand), Reilinger et al. (2000); Duman et al. (2003); 12: 2001 Kunlun, Lassere et al. (2005); Xu et al. (2006); 13: 2002 Denali, Wright et al. (2004); Haeussler et al. (2004a); 14: 2002 Denali, Elliott et al. (2007); Haeussler et al. (2004a). Black rectangles show percentage of off-fault deformation measured by Shelef and Oskin (2010) from the Calico (C) and Harper Lake (H) faults in the eastern California shear zone, respectively, expressed as LSSR ratios. Note that the 31–46% range for off-fault deformation observed on the Harper Lake fault is a minimum; the actual amount of distributed deformation in this example is likely larger (Shelef and Oskin, 2010), and thus the LSSR will be even lower than shown here.

the LSSR results reveal a clear correlation between the progressive localization of fault slip at the surface and increasing cumulative fault displacement, for both structurally simple and structurally complex sections of the fault traces (Fig. 3). For example, the low LSSR values (∼0.6) for the small-cumulative-displacement (3–4 km) faults that ruptured during the 1992 M_w 7.3 Landers and 1999 M_w 7.1 Hector Mine earthquakes indicate significant near-surface distributed deformation, even along the straight, continuous, structurally simple sections of these surface ruptures (i.e., ∼40% of the total slip at depth did not reach the surface along a narrow, localized fault trace for three of the four main faults involved in these ruptures). In contrast, the LSSR values for structurally simple parts of the surface ruptures along faults with larger cumulative displacements are systematically larger, with typical LSSR values of ∼0.8–0.9 for faults with ⩾∼85 km of cumulative slip. Interestingly, the LSSR values appear to saturate at ∼85 km of cumulative fault slip, although more data from other large earthquakes on structurally mature faults are needed to verify and refine this observation.

the methods employed by different researchers in the inversion process (cell size, cell depth distribution, choice of smoothing parameters, number of interferograms used, addition [or not] of GPS data and surface geological slip data as constraints, availability [or not] of GPS and surface slip data, and when available, the density of such observations) preclude assignment of consistent formal error estimates for the inversion slip data. This problem is at least partially ameliorated by our use of multiple inversions by different groups wherever possible.

It is worth noting that even these LSSR values may be slightly overestimated. Specifically, Barbot et al. (2008) demonstrated that failure to include a mechanically compliant zone at the fault in models of co-seismic deformation patterns will result in underestimation of slip at depth in geodetically constrained inversions. This problem is negligible over much of the co-seismic depth range, but could be as much as 20% at ∼3 km depth. Thus, in the depth range of interest in this study, the fact that the inversions used for our comparison did not incorporate mechanically compliant zones indicates that they likely slightly underestimate the amount of slip at depth. Consequently, our comparisons of those values with measurements of slip at the fault trace will yield a slight (⩽20%) underestimate of the LSSR.

4. Discussion

4.1. Is the shallow slip deficit accommodated by distributed near-surface deformation or interseismic fault creep?

As noted above, multiple analyses show that in general co-seismic fault slip at the surface is less than slip at depth. Yet total slip at the surface must equal total slip at depth over multiple earthquake cycles. The question therefore arises, how is this "missing" shallow slip accommodated? Is this deficit caused by distributed deformation around "the fault", or is it accommodated by aseismic fault creep on the shallowest parts of the fault during the interseismic period?

Observations from numerous recent surface ruptures document significant off-fault distributed co-seismic surface deformation, even along some parts of ruptures on structurally mature faults (e.g., Akyuz et al., 2002; Hartleb et al., 2002; Rockwell et al., 2002; Treiman et al., 2002; Duman et al., 2003; Liu et al., 2003; Xu et al., 2006). In the extreme case where a large-magnitude rupture extends upwards through relatively homogeneous, previously un-ruptured materials, even surface displacements as large as several meters can occur almost entirely by distributed deformation, with little to no discrete faulting, as occurred during the 2010 M_w 7.1 Darfield earthquake (Van Dissen et al., 2011). Thus, it seems likely that much of the apparent shallow slip deficit is accounted for by shallow, off-fault distributed deformation.

A possible alternative explanation is that the shallow slip deficit is made up by fault creep that occurs during the interseismic period. Interseismic near-surface fault creep has been documented for a number of continental strike-slip faults (e.g., Allen, 1968; Savage and Burford, 1973; Schulz et al., 1982; Allen et al., 1991; Bilham et al., 2004; Çakir et al., 2003, 2012; Karabacak et al., 2011; Lienkaemper et al., 2012; Kaneko et al., 2013; Lindsey et al., in press), and any such creep would help to fill in the "missing" shallow slip documented in the six earthquakes we discuss above. But to explain the correspondence we observe between fault structural maturity and the ratio of co-seismic fault slip at the surface versus slip at depth would require that interseismic surface fault creep occurs preferentially on structurally immature faults (i.e., those that exhibit low SSR values). Yet most well-documented examples of significant interseismic fault creep come from structurally mature to super-mature faults, such as the various creeping strands of the San Andreas fault system, the Xianshuihe fault, and the North Anatolian fault (e.g., Allen, 1968; Allen et al., 1991; Çakir et al., 2005, 2012; Bilham et al., 2004; Karabacak et al., 2011; Lienkaemper et al., 2012; Kaneko et al., 2013; Lindsey et al., in press). It is possible that this is because these mature faults have faster slip rates than many less-mature faults, and thus the creep is more readily detectable with geodetic data. However, both the Landers and Hector Mine ruptures exhibited only minor post-seismic fault creep, and neither was followed by detectable interseismic shallow fault creep (Jacobs et al., 2002;

Fialko, 2004). Similarly, Çakir et al. (2012) analysis of post-seismic geodetic data from the 1999 M_w 7.5 Izmit earthquake shows that whereas post-seismic surface creep has been occurring at rapid rates (approximately the full fault slip rate) for more than a decade on the structurally mature main [Izmit] strand of the NAF, no creep is occurring on the less-mature Karadere strand (85 km vs. 25 km of total slip, respectively; Armijo et al., 1999). To explain this, we suggest that it is also possible that in addition to the presence of velocity-strengthening materials in the fault zone (e.g., Allen, 1968; Scholz, 2002), creep is enhanced by the development through progressive strain localization of a narrow, high-strain fault core that extends all the way to the surface. Additional studies of the possibility of slow interseismic creep on structurally immature faults will be required to determine what role, if any, progressive localization of shallow faulting on structurally mature faults plays in facilitating fault creep. However, even if shallow interseismic fault creep is detected at rates approaching the full fault slip rate following future earthquakes on structurally immature faults, the absence of any such interseismic creep along the faults that ruptured in the Landers and Hector Mine earthquakes and the Karadere strand of the Izmit rupture demonstrates that this cannot be the sole explanation for the shallow slip deficit.

We thus consider it unlikely that interseismic fault creep can explain the correlation we observe between small cumulative fault displacements and low SSR and LSSR values. Rather, we suggest that most of the shallow slip deficit is accommodated by distributed near-surface deformation, and that much of that likely occurs co-seismically or during the early, rapid post-seismic period that is encompassed in most of the geologic and geodetic measurements described above. This type of behavior has previously been suggested on the basis of dynamic rupture propagation models that include depth-dependent stress increases and inelastic off-fault yielding (e.g., Ma, 2008; Ma and Andrews, 2010).

4.2. Implications for structural evolution of fault zones

The consistency of the correlation between surface slip localization and cumulative fault slip shown in Fig. 3 suggests that the individual-earthquake data we use for the LSSR comparisons provide a good representation of the overall, longer-term pattern of fault slip at the surface. This inference is supported by other evidence for progressive slip localization from analysis of long-term patterns of distributed slip on other faults. For example, Shelef and Oskin (2010) mapped the deformation of relatively linear geologic features that have been offset by two faults in the Mojave Desert of California. Their mapping on the Calico fault, which has 9.6 km of cumulative fault slip, shows that ~23% of the total right-lateral shear this fault has experienced occurred as off-fault, distributed deformation. On the nearby Harper Lake fault, which has only 3.5 km of total fault slip, they showed that at least 31–46% of the total shear occurred via off-fault deformation. As shown in Fig. 3, these values plot along the trend of our LSSR data for faults with small cumulative displacement, suggesting that our LSSR results record a basic feature of fault-zone evolution, rather than an artifact of our comparison of the disparate geologic (site specific) and geodetic (spatially averaged) data sets we used in our comparisons. Moreover, it is worth noting that the off-fault strain measured by Shelef and Oskin (2010) along the Calico and Harper Lake faults is the cumulative total off-fault strain in bedrock since inception of the faults. Inasmuch as these faults may have undergone some exhumation, the observation in this study that fault localization apparently increases with depth suggests that the Shelef and Oskin (2010) estimates may actually underestimate the total amount of off-fault strain accommodated at the surface during individual earthquakes.

These observations support the long-held idea that strain is progressively localized along faults during increasing cumulative displacement (e.g., Tchalenko, 1970; Segall and Pollard, 1983; Zhang et al., 1989; Vermilye and Scholz, 1998; Wesnousky, 1988; Stirling et al., 1996; Evans et al., 2000; Manighetti et al., 2001, 2004; Chester et al., 2004; Frost, et al., 2009). In the upper few kilometers of the crust, faults are typically surrounded by mechanically compliant “damage zones” characterized by reduced seismic velocities (e.g., Chester and Logan, 1986; Li et al., 1994, 1998, 1999, 2004; Ben-Zion, 1998; Fialko et al., 2002; Ben-Zion and Sammis, 2003; Ben-Zion et al., 2003; Peng et al., 2003; Fialko, 2004; Li et al., 2004; Cochran et al., 2006, 2009; Hamiel and Fialko, 2007; Barbot et al., 2008; Ma, 2008; Ma and Andrews, 2010; Shelef and Oskin, 2010). The total width of these zones (1–2 km) appears to be similar for both structurally immature faults, such as those that ruptured in the Landers and Hector Mine earthquakes, and structurally mature faults, such as the San Andreas. Such data suggest to us that the damage zones along mature faults are likely largely relict features that developed early in the fault’s history and were subsequently abandoned as slip progressively localized on to the main fault strand. This inference is supported by a recent study of an exhumed, structurally mature (>65 km displacement) strike-slip fault in the eastern Alps, in which Frost et al. (2009) demonstrated that the >200-m-wide damage zone developed early, and was effectively “fossilized” as slip became progressively localized onto a high-strain fault core of <10 m width.

Based on these observations, we suggest that the trends evident in the LSSR data described above are a manifestation of progressive localization of slip onto the main fault strand all the way to the surface. For example, along structurally immature faults, such as those that ruptured in the 1992 Landers and 1999 Hector Mine earthquakes, the generally low LSSR values, even along structurally simple, straight parts of the rupture trace, suggest that strain has not yet completely localized onto a narrow high-strain fault core, and that significant strain is still being accommodated outside the fault core within the surrounding damage zone. This is consistent with the suggestion of Shelef and Oskin (2010) that the development of the distributed deformation they observe around the Mojave faults they examined is an ongoing process. In contrast, the structurally simple sections of the more structurally mature faults that we examined generally exhibit high LSSR values indicative of strain localization all the way to the surface.

4.3. Implications for strong ground motion effects

The degree to which localization of fault-zone structure (or lack thereof) all of the way up to the earth’s surface controls strong ground motions remains poorly understood, largely because of the dearth of strong ground motion records from near large strike-slip earthquakes. Nevertheless, it is possible that the differing percentages of on- versus off-fault slip could affect the spatial distribution, frequency content, and magnitude of strong ground motions in future earthquakes on faults of differing structural maturity. Such differences, which could potentially be anticipated in advance of future earthquakes, could contribute to more accurate predictions of strong ground motion effects in future earthquakes.

For example, engineered buildings and other infrastructure designed to react to an earthquake may experience a different response if the fault-zone deformation is more rather than less localized. Similarly, stress drops and ground motion frequency content may vary depending on the structural maturity of the fault, and the amount of on-fault vs. off-fault deformation. For example, rupture to the surface through velocity-strengthening materials will consume energy and slow the rupture, reducing ground motions in the frequency range of most interest to structural engineers

(e.g., Brune and Anooshehpoor, 1998; Day and Ely, 2002; Sammis et al., 2009; Bhat et al., 2010, 2012; Biegel et al., 2010; Kaneko and Fialko, 2011). Although such behavior may affect even structurally mature faults (e.g., San Andreas), the larger percentage of distributed near-surface slip that occurs during earthquakes on structurally immature faults may amplify this effect, yielding significantly different ground motions than would be expected for a similar rupture on a more mature fault. Complicating this picture is the fact that slip along structurally complex parts of the faults, such as might be expected to occur more commonly along structurally immature faults (Wesnousky, 1988; Stirling et al., 1996), could generate locally large high-frequency motions (e.g., Oglesby and Mai, 2012), but could also reduce the ground motion amplifying effects of directivity (Lozos et al., 2013). In addition to detailed observations of patterns of strong ground motions in future earthquakes, comparisons of ground motions generated by ruptures on faults of varying structural maturity could help to elucidate the degree to which the amount of on- vs. off-fault surface deformation controls patterns of strong ground motions.

4.4. Implications for the interpretation and use of geologic fault slip rates in analysis of seismic hazard and patterns of plate boundary deformation

These observations have important implications for our understanding and interpretation of geologic slip rates. Specifically, these results indicate that, on average, the structurally simple parts of structurally mature, large-cumulative-slip faults will be more likely to yield slip rates that are more representative of the true fault slip rate, because strain along such faults has more fully localized onto a narrow, high-strain fault core all the way to the surface. Even in such situations, however, some strain may remain distributed outside of the fault core. For example, comparison of the amount of off-fault distributed surface deformation measured by Rockwell et al. (2002) after the 1999 Izmit rupture reveals several locations where as much as 25–40% of the total deformation was distributed off-fault (almost all within a few meters to a few tens of meters from the fault trace). Thus, even rates derived from structurally simple parts of structurally mature fault should probably considered minima, possibly by as much as ∼10–20%. It is worth noting, however, that there are two main types of geologic slip-rate study, one that restores offset geomorphic features (e.g., stream terraces), and another that traces buried depositional features (e.g., distinctive stream channel deposits) through a series of three-dimensional trench exposures all the way to the fault. Such 3-D trench studies reveal the detailed distribution of slip along and adjacent to the main fault zone in exceptional detail, but are commonly (not always) localized to within a few meters of the fault because of the labor-intensive nature of such work. In the context of the observations above, we echo Kozaci et al. (2007, 2009) in suggesting that it is much more likely that slip-rate studies of large geomorphic offsets, which may encompass the majority of off-fault, near-surface distributed deformation (much of which occurs within a few meters of the fault; e.g., Rockwell et al., 2002) may be more likely to yield a total slip rate reflective of the true slip rate at depth than short-aperture measurements derived from 3-D trench studies.

The low LSSR values for faults with small cumulative displacements (<25 km) suggest that strain has not yet completely localized onto a narrow high-strain fault-zone core, even along structurally simple, straight parts of the fault trace, and that significant strain is still being accommodated outside the fault core within the surrounding damage zone. Thus, slip-rate measurements for low-cumulative slip faults (e.g., those of the Mojave section of the eastern California shear zone; Oskin et al., 2008) will probably yield apparent rates that are much slower than the actual "slip rate" of the seismogenic part of the fault at depth (by perhaps 30–40%). This has obvious implications for the use of such rates in probabilistic seismic hazard assessments, many of which depend on geologic slip rates as a basic model input. Specifically, consistent underestimation of the slip rates of structurally immature, small-cumulative-displacement faults will yield earthquake probability assessments for these faults, and indeed for any regions containing such faults, that may not properly account for the overall strain being accommodated by these structures.

These observations will also have an impact on models of continental deformation that use late Quaternary slip rates to examine patterns of regional deformation (e.g., Avouac and Tapponnier, 1993; Humphreys and Weldon, 1994; England and Molnar, 1997; Bird, 2009; Loveless and Meade, 2011). Specifically, studies that sum fault slip rates as a check on models designed to examine the degree to which continental deformation occurs via distributed, quasi-continuous deformation versus localized fault displacement in continents will underestimate the importance of fault slip relative to more distributed deformation. We note, however, that this effect will likely be relatively small (⩽∼10–20%) for regions dominated by slip on structurally mature, large-cumulative-displacement faults (e.g., the Altyn Tagh and Kunlun faults in central Asia; North Anatolian fault in Turkey; San Andreas fault in California; Denali fault in Alaska). In contrast, the effect is likely to be quite significant in regions dominated by structurally immature, small-cumulative-displacement faults such as the eastern California shear (ECSZ)-Walker Lane belt in the western USA (e.g., Frankel et al., 2011).

Our results are also important for accurate determination of paleo-magnitudes for earthquakes that occurred before the seismograph era. Specifically, if these estimates are based on surface displacements, either from regressions of surface slip-vs.-M_w or from a combination of surface slip, estimated rupture length, and an assumed rupture depth (usually assumed to be the base of microseismicity, but see King and Wesnousky, 2007, for additional discussion), the occurrence of any near-surface distributed deformation will result in an underestimate of the true moment-magnitude. Given the systematic relationship between the degree to which these measurements will underestimate total slip at depth and cumulative slip documented in this study, such underestimates will likely be greater for earthquakes that occurred on structurally less-mature faults. In contrast, although estimates for paleo-earthquakes on structurally mature faults, such as the San Andreas and North Anatolian faults (e.g., Sieh, 1978; Barka, 1996), will underestimate slip at depth, the error will be relatively smaller.

4.5. Implications for comparison of geologic and geodetic rate data

Similarly, these observations have significant implications for comparisons of short-term geodetic measurements, which record the entire rate of interseismic elastic strain accumulation on a fault, with longer-term geologic slip rates, which record the cumulative displacement averaged over many earthquake cycles, in the search for regions of transiently elevated or reduced rates of elastic strain accumulation and release. For example, it has been suggested that the Mojave section of the ECSZ may be storing elastic strain energy at a rate that is much faster than its rate of strain release (Peltzer et al., 2001; Oskin and Iriondo, 2004; Dolan et al., 2007; Oskin et al., 2008; McGill et al., 2009; Ganev et al., 2010). Specifically, the cumulative geologic slip rate of the six main faults that comprise the ECSZ in the Mojave is 6.2 ± 1.9 mm/yr (Oskin et al., 2008), whereas geodetic measurements, including those made before the 1992 M_w 7.3 Landers earthquake, indicate elastic strain accumulation at a rate of 12 ± 2 mm/yr (Savage et al., 1990; Sauber et al., 1994; Dixon et al., 1995; Gan et al., 2000;

Bennett et al., 2003; Meade and Hager, 2005). Thus, the fault network has appeared to be storing energy at a rate that is almost twice as fast as its long-term average. But the geologic slip rates upon which this comparison rests all come from structurally immature faults with displacements ranging from 2–10 km (Jachens et al., 2002). The comparisons described in this paper suggest that these rates probably underestimate the true slip rates of these faults by as much as 40%, indicating a true cumulative slip rate across the entire ECSZ that is much closer to the geodetically defined rate of elastic strain accumulation. Addition of this "missing" component of distributed surface deformation to the measured slip rates would therefore suggest that geologic and geodetic rates may approximately match. This would in turn suggest that there is no transiently elevated accumulation of elastic strain in this part of the ECSZ. For example, addition of 30% off-fault distributed deformation (the low end of our estimates above) to the cumulative on-fault ECSZ slip rate of Oskin et al. (2008) yields a revised total ECSZ geologic displacement rate of 8.1 ± 2.5 mm/yr. Moreover, the rate of elastic strain accumulation inferred across the Mojave region is highly dependent on strain accumulation associated with the San Andreas fault (see discussion of this issue in Lindsey and Fialko, 2013). Specifically, consideration of non-vertical SAF geometries may give rise to a total geodetic strain accumulation rate across the Mojave region that is somewhat slower than the commonly cited value of 12 ± 2 mm/yr (Fialko and Rivet, 2008), similar to our revised ECSZ-wide cumulative fault displacement rate. These observations suggest that it is unlikely that there is a transiently elevated rate of accumulation of elastic strain in this part of the ECSZ. We note, however, that all of these values have relatively large error bars, and although we think it is unlikely that a 2:1 strain transient exists in the Mojave, it is of course possible that a more subtle transient still exists. But the data do not appear to require this.

4.6. The importance of near-surface geologic materials

Although the observations described above point to fault structural maturity as a first-order control on localization (or lack thereof) at the surface, other factors likely also control the relative importance of on- versus off-fault slip. Perhaps the most obvious of these potential additional controls is the type of near-surface material through which the fault ruptures (e.g., Ma, 2008; Ma and Andrews, 2010; Kaneko and Fialko, 2011).

Examples from recent earthquakes suggest that sections of a fault that rupture upwards through bedrock all the way to the surface will exhibit more localized strain, and therefore higher LSSR values. For example, in the 1999 Hector Mine earthquake, the 10-km-long section of the surface rupture that extended through bedrock in the Bullion Mountains exhibited the largest displacements observed in that earthquake (Treiman et al., 2002). Comparison with the inversion results of Simons et al. (2002) and Jónsson et al. (2002) reveals LSSR values of $\sim$0.8 to >1 for this stretch of the fault, relative to values outside the zone of bedrock rupture that are mostly $\leqslant$0.6.

There are other examples, however, of low LSSR values along stretches of fault that extend through bedrock at the surface. For example, along central part of Karadere segment of the 1999 M_w 7.5 Izmit rupture, the average LSSR value is only 0.75–0.80, despite the fact that this part of the Izmit surface rupture extended through bedrock up the surface for most of its length. In this case, at least, the structural complexity of the structurally immature Karadere strand appears to dominate over the effect of bedrock geology, through which the fault cuts all the way to the surface.

Conversely, the presence of exceptionally thick and/or previously undeformed sediments in the near-surface can lead to delocalization of surface slip. As noted above, an extreme example of this phenomenon occurred during the 2010 M_w 7.0 Darfield, New Zealand, earthquake. This rupture extended for more than 30 km with an average surface slip of 2.5 m, and a maximum slip of 5 m (Van Dissen et al., 2011). Despite these large surface displacements, there was essentially no discrete fault trace. Rather, deformation along the entire rupture was spread over a 30- to 300-m-wide zone of distributed deformation. Van Dissen et al. (2011) attributed this behavior to the presence of very thick sequence of glacial outwash gravels. Although a cumulative displacement on this fault is not yet known, the absence of previous geomorphic expression, coupled with the structurally complex fault geometry (e.g., Duffy et al., 2013), suggests that it is a slow-moving, structurally immature fault. Thus, in extreme cases of structurally immature faults extending to the surface through previously undeformed thick sediments, the LSSR can be close to zero, even on faults capable of generating relatively large-magnitude earthquakes such as the 2010 Darfield event. We emphasize, however, that this example is extreme, and in the six large-magnitude earthquakes described above ruptures extending across previously deformed sediments exhibited significant surface rupture that was controlled in large part by the structural maturity of the fault. Nevertheless, additional measurements of LSSR relative to fault structurally maturity and the thickness and types of near-surface materials will be required to assess the relative importance of these two effects.

5. Conclusions

Our comparisons of geological surface displacements with geodetically constrained inversions for slip at depth in six large ($M_w \geqslant 7.1$) strike-slip earthquakes reveal a consistent correlation between fault structural maturity and the percentage of total surface displacement that occurs on narrow zones of surface rupture relative to more distributed deformation. Specifically, only $\sim$50–60% of the total surface deformation in earthquakes on structurally immature fault zones ($\leqslant\sim$25 km of total displacement) is localized at the fault trace, whereas $\sim$85–95% of the total surface slip occurs at the fault trace on mature faults. If the data from these six earthquakes are representative of the long-term patterns of surface deformation, and the consistency of the patterns spanning a large number of earthquakes and a wide range of magnitude suggests that they are, then geologic slip rates based on repeated such surface ruptures will underestimate the actual slip rate of the faults at seismogenic depths.

This observation is of fundamental importance for a wide range of studies, perhaps most especially for probabilistic seismic hazard analysis (PSHA), which uses such rates as a basic input to renewal models. If geologic slip rates are consistently underestimated, then the resulting earthquake probability estimates will also be underestimated. This issue may affect all slip rates, although it is likely to be much more significant for structurally immature faults than for large, mature strike-slip faults such as the San Andreas fault in California. Similarly, these results are important for comparisons of short-term interseismic geodetic data with longer-term geologic rates in the search for strain transients. If fault slip rates are underestimated, then differences with geodetic rates suggestive of accelerated strain accumulation may be overestimated. This appears to be the case for the hypothesized transient in the Mojave section of the eastern California shear zone, which we suggest is largely an artifact of underestimation of geologic slip rates and possibly overestimation of geodetically constrained rates of elastic strain accumulation.

Systematic underestimation of geologic slip rates will also have an impact on studies that use these data to determine the relative importance of on-fault versus distributed deformation in continental settings, as well as for the estimation of paleo-magnitudes in pre-instrumental era earthquakes. The degree to which fault slip

remains localized all the way to the surface will also affect the response of buildings built on or near faults, and should be considered accordingly in design criteria. The implications of these results for the prediction of strong ground motion effects remain unclear, as the relationship between on- versus off-fault deformation and ground motion patterns remains incompletely understood. Future determinations of on-fault versus off-fault deformation on other large-magnitude earthquake surface ruptures will yield the larger database necessary to develop statistical measures of the localization of slip at the surface on the basis of measurable fault parameters, such as cumulative fault slip, and the as-yet-poorly understood role played by the type of near-surface geological materials through which surface ruptures extend.

Acknowledgements

We thank Manuel Berberian, Rob Graves, Yuri Fialko, Jeff Freymueller, Peter Haeussler, Liz Hearn, Yann Klinger, Rowena Lohman, David Oglesby, Rob Reilinger, Charlie Sammis, Wayne Thatcher, and Tim Wright for helpful discussions and sharing of data. Ruth Harris, James Hollingsworth, and an anonymous reviewer provided constructive comments of the manuscript. This research was supported by the Southern California Earthquake Center (SCEC) and the US National Science Foundation (NSF EAR-1147436). SCEC is funded by NSF Cooperative Agreement EAR-0106924 and USGS Cooperative Agreement 02HQAG0008.

Appendix A. Supplementary material

Supplementary material related to this article can be found online at http://dx.doi.org/10.1016/j.epsl.2013.11.043.

References

Akyuz, S., Hartleb, R., Altunel, E., Sunal, G., Meyer, B., Armijo, R., 2002. Surface rupture and slip distribution of the 12 November 1999 Duzce earthquake (M 7.1), North Anatolian fault, Bolu, Turkey. Bull. Seismol. Soc. Am. 92, 61–66.

Allen, C.R., 1968. The tectonic environments of seismically active and inactive areas along the San Andreas fault system. In: Dickinson, R., Grantz, A. (Eds.), Proceedings of Conference on Geologic Problems of the San Andreas Fault System. In: Stanf. Univ. Publ. Geol. Sci., vol. 11, pp. 70–82.

Allen, C.R., Luo, Z., Qian, H., Wen, X., Zhou, H., Huang, W., 1991. Field study of a highly active fault zone: The Xianshuihe fault of southwestern China. Geol. Soc. Am. Bull. 103, 1178–1199.

Armijo, R., Meyer, B., Hubert, A., Barka, A., 1999. Westward propagation of the North Anatolian fault into the northern Aegean: Timing and kinematics. Geology 27 (3), 267–270.

Avouac, J.-P., Tapponnier, P., 1993. Kinematic model of active deformation in central Asia. Geophys. Res. Lett. 20, 895–898.

Ayoub, F., Leprince, S., Avouac, J.P., 2009. Co-registration and correlation of aerial photographs for ground deformation measurements. ISPRS J. Photogramm. Remote Sens. 64 (6), 551–560.

Barbot, S., Fialko, Y., Sandwell, D., 2008. Effect of a compliant fault zone on the inferred earthquake slip distribution. J. Geophys. Res. 113, B06404. http://dx.doi.org/10.1029/2007JB005256.

Barka, A.A., 1996. Slip distribution along the North Anatolian fault associated with large earthquakes of the period 1939–1967. Bull. Seismol. Soc. Am. 86 (5), 1238–1254.

Bennett, R.A., Wernicke, B.P., Niemi, N.A., Friedrich, A.M., Davis, J.I., 2003. Contemporary strain rates in the northern Basin and Range province from GPS data. Tectonics 22 (2), 1008. http://dx.doi.org/10.1029/2001TC001355.

Benowitz, J.A., Layer, P.W., Armstrong, P., Perry, S.E., Haeussler, P.J., Fitzgerald, P.G., VanLaningham, S., 2011. Spatial variations in focused exhumation along a continental-scale strike-slip fault: The Denali fault of the eastern Alaska Range. Geosphere 7 (2), 1–13.

Ben-Zion, Y., 1998. Properties of seismic fault zone waves and their utility for imaging low velocity structures. J. Geophys. Res. 103, 12567–12585.

Ben-Zion, Y., Sammis, C.G., 2003. Characterization of fault zones. Pure Appl. Geophys. 160, 677–715.

Ben-Zion, Y., Peng, Z., Okaya, D., Seeber, L., Armbruster, J.G., Ozer, N., Michael, A.J., Baris, S., Aktar, M., 2003. A shallow fault zone structure illuminated by trapped waves in the Karadere–Duzce branch of the north Anatolian Fault. Geophys. J. Int. 152, 699–717.

Berberian, M., Jackson, J.A., Qorashi, M., Khatib, M.M., Priestly, K., Talebian, M., Ghafuri-Ashtiani, M., 1999. The 1997 May 10 Zirkuh (Qa'enat) earthquake (M_w 7.2): faulting along the Sistan suture zone of eastern Iran. Geophys. J. Int. 136, 671–694.

Bhat, H.S., Biegel, R.L., Rosakis, A.J., Sammis, C.G., 2010. The effect of asymmetric damage on dynamic shear rupture propagation II: With mismatch in bulk elasticity. Tectonophysics 493, 263–271. http://dx.doi.org/10.1016/j.tecto.2010.03.016.

Bhat, H.S., Rosakis, A.J., Sammis, C.G., 2012. A micromechanics based constitutive model for brittle failure at high strain rates. J. Appl. Mech. 79 (3), 031016. http://dx.doi.org/10.1115/1.4005897.

Biegel, R.L., Bhat, H.S., Sammis, C.G., Rosakis, A.J., 2010. The effect of asymmetric damage on dynamic shear rupture propagation I: No mismatch in bulk elasticity. Tectonophysics 493, 254–262. http://dx.doi.org/10.1016/j.tecto.2010.03.020.

Bilham, R., Suszek, N., Pinkney, S., 2004. California Creepmeters. Seismol. Res. Lett. 75 (4), 481–492. http://dx.doi.org/10.1785/gssrl.75.4.481.

Bird, P., 2009. Long-term fault slip rates, distributed deformation rates, and forecast of seismicity in the western United States from joint fitting of community geologic, geodetic, and stress direction data sets. J. Geophys. Res. 114, B11403.

Brune, J.N., Anooshehpoor, A., 1998. A physical model of the effect of a shallow weak layer on strong ground motion for strike-slip ruptures. Bull. Seismol. Soc. Am. 88, 1070–1078.

Çakir, Z., de Chabalier, J.-B., Armijo, R., Meyer, B., Barka, A., Peltzer, G., 2003. Coseismic and early postseismic slip associated with the 1999 Izmit earthquake (Turkey), from SAR interferometry and tectonic field observations. Geophys. J. Int. 155, 93–110.

Çakir, Z., Akolglu, A.M., Belabbes, S., Ergintav, S., Meghraoui, M., 2005. Creeping along the Izmetpasa section of the North Anatolian fault (western Turkey): Rate and extent from InSAR. Earth Planet. Sci. Lett. 238, 225–234. http://dx.doi.org/10.1016/j.epsl.2005.06.044.

Çakir, Z., Ergintav, S., Haluk, Ö., Dogan, U., Akoglu, A.M., Meghraoui, M., Reilinger, R., 2012. Onset of aseismic creep on major strike-slip faults. Geology 40, 1115–1118. http://dx.doi.org/10.1130/G33522.1.

Chester, F.M., Logan, J.M., 1986. Implications for mechanical properties of brittle faults from observations of the Punchbowl fault zone, California. Pure Appl. Geophys. 124, 79–106.

Chester, F.M., Chester, J.S., Kirschner, D.L., Schulz, S.E., Evans, J.P., 2004. Structure of large-displacement strike-slip fault zones in the brittle continental crust. In: Karner, G.D., Taylor, B., Driscoll, N.W., Kohlstedt, D.L. (Eds.), Rheology and Deformation in the Lithosphere at Continental Margins. In: MARGINS Theor. Exp. Earth Sci. Ser., vol. 1. Columbia Univ. Press, New York, pp. 223–260.

Cochran, E.S., Radiguet, M., Shearer, P.M., Li, Y.-G., Fialko, Y., Vidale, J.E., 2006. Seismic imaging of the damage zone around the Calico Fault. Eos Trans. AGU 87 (52). Suppl., abst. T23E-03.

Cochran, E., Li, Y.-G., Shearer, P.M., Barbot, S., Fialko, Y., Vidale, J., 2009. Seismic and geodetic evidence for extensive, long-lived fault damage zones. Geology 37 (4), 315–318. http://dx.doi.org/10.1130/G25306A.1.

Day, S.M., Ely, G.P., 2002. Effect of a shallow weak zone on fault rupture: numerical simulation of scale-model experiments. Bull. Seismol. Soc. Am. 92, 3022–3041.

Dixon, T.H., Robaudo, S., Lee, J., Reheis, M.C., 1995. Constraints on present-day Basin and Range deformation from space geodesy. Tectonics 14, 755–772.

Dolan, J.F., Bowman, D.D., Sammis, C.G., 2007. Long-range and long-term fault interactions in Southern California. Geology 35 (9), 855–858.

Duffy, B., Quigle, M., Barrel, D.J.A., Van Dissen, R., Stahl, T., Leprince, S., McInnes, C., Bilderback, E., 2013. Fault kinematics and surface deformation across a releasing bend during the 2010 M_W 7.1 Darfield, New Zealand, earthquake revealed by differential LiDAR and cadastral surveying. Geol. Soc. Am. Bull. 125 (3/4), 420–431. http://dx.doi.org/10.1130/B30753.1.

Duman, T.Y., Awata, Y., Yoshikazu, T., Emre, Ö., Dogan, A., Özalp, S., 2003. Surface rupture associated with the August 17, 1999 Izmit earthquake. In: Emre, Ö., Awata, Y., Duman, T.Y. (Eds.), Special Publication Series 1, Appendix 1 (Surface Rupture Maps and Slip Measurements). General Directorate of Mineral Research and Exploration (Maden Tetkik ve Arama Genel Müdürlügü [MTA]), Ankara, Turkey, pp. 57–86.

Eisbacher, G.H., 1976. Sedimentology of the Dezadeash flysch and its implications for strike-slip faulting along the Denali fault, Yukon Territory and Alaska. Can. J. Earth Sci. 13, 1495–1513.

Elliott, J., Freymueller, J.T., Rabus, B., 2007. Coseismic deformation of the 2002 Denali Fault earthquake: Contributions from SAR range offsets. J. Geophys. Res. 112, B06421. http://dx.doi.org/10.1029/2006JB004428.

England, P., Molnar, P., 1997. The field of crustal velocity in Asia calculated from Quaternary rates of slip on faults. Geophys. J. Int. 130, 551–582.

Evans, J.P., Shipton, Z.K., Pachell, M.A., Lim, S.J., Robeson, K., 2000. The structure and composition of exhumed faults, and their implication for seismic processes. In: Bokelmann, G., Kovach, R.L. (Eds.), Proceedings of the 3rd Conference on Tectonic Problems of the San Andreas System. Stanford University, pp. 67–81.

Fialko, Y., 2004. Evidence of fluid-filled upper crust from observations of postseismic deformation due to the 1992 M_W 7.3 Landers earthquake. J. Geophys. Res. 109, B08401. http://dx.doi.org/10.1029/2004JB002985.

Fialko, Y., Rivet, D., 2008. Secular and transient deformation in the Eastern California shear zone from InSAR and GPS observations over 1992–2007 epoch. Eos Trans. AGU 89 (23). Jt. Assem. Suppl., Abstract G33B-01.

Fialko, Y., Sandwell, D., Agnew, D., Simons, M., Shearer, P., Minster, B., 2002. Deformation on nearby faults induced by the 1999 Hector Mine earthquake. Science 297, 1858–1862.

Fialko, Y., Sandwell, D., Simons, M., Rosen, P., 2005. Three-dimensional deformation caused by the Bam, Iran, earthquake and the origin of shallow slip deficit. Nature 435, 295–299. http://dx.doi.org/10.1038/nature03425.

Frankel, K.L., Dolan, J.F., Owen, L.A., Ganev, P., Finkel, R.C., 2011. Spatial and temporal constancy of seismic strain release along an evolving segment of the Pacific–North America plate boundary. Earth Planet. Sci. Lett. 304, 565–576.

Frost, E., Dolan, J.F., Sammis, C.G., Hacker, B.R., Cole, J., Ratschbacher, L., 2009. Progressive strain localization in a major strike-slip fault exhumed from midseismogenic depths: Structural observations from the Salzach–Ennstal–Mariazell-fault system, Austria. J. Geophys. Res. 114, B04406. http://dx.doi.org/10.1029/2008JB005763.

Fu, B., Awata, Y., 2007. Displacement and timing of left-lateral faulting in the Kunlun Fault Zone, northern Tibet, inferred from geologic and geomorphic features. J. Asian Earth Sci. 29, 253–265. http://dx.doi.org/10.1016/j.jseaes.2006.03.004.

Gan, W., Svarc, J.L., Savage, J.C., Prescott, W.H., 2000. Strain accumulation across the Eastern California shear zone at latitude 36°30′N. J. Geophys. Res. 105, 16229–16236.

Ganev, P.N., Dolan, J.F., Oskin, M., Blisniuk, K., Owen, L.A., 2010. Paleoseismologic evidence for multiple Holocene earthquakes on the Calico fault: Implications for earthquake clustering in the Eastern California Shear Zone. Lithosphere 2 (4), 287–298. http://dx.doi.org/10.1130/L82.1. Data Repository 2010217.

Haeussler, P.J., Schwartz, D.P., Dawson, T.E., Stenner, H.D., Lienkaemper, J.J., Sherrod, B., Cinti, F.R., Montone, P., Craw, P., Crone, A.J., Personius, S.F., 2004a. Surface rupture and slip distribution of the Denali and Totschunda Faults in the 3 November 2002 M 7.9 earthquake, Alaska. Bull. Seismol. Soc. Am. 94, S23–S52.

Haeussler, P.J., Schwartz, D.P., Dawson, T.E., Stenner, H.D., Lienkaemper, J.J., Cinti, F.R., Montone, P., Sherrod, B., Craw, P., 2004b. Surface rupture of the 2002 Denali Fault, Alaska, earthquake and comparison with other strike-slip ruptures. Earthq. Spectra 20, 565–578.

Hamiel, Y., Fialko, Y., 2007. Structure and mechanical properties of faults in the North Anatolian fault system from InSAR observations of coseismic deformation due to the 1999 Izmit (Turkey) earthquake. J. Geophys. Res. 112, B07412. http://dx.doi.org/10.1029/2006JB004777.

Hartleb, R.D., Dolan, J.F., Akyüz, S., Dawson, T.E., Tucker, A.Z., Yerli, B., Rockwell, T.K., Toraman, E., Çakir, Z., Dikbas, A., Altunel, E., 2002. Surface rupture and slip distribution along the Karadere segment of the 17-August-1999 Izmit, Turkey, earthquake. Bull. Seismol. Soc. Am. 92, 67–78. Special Issue on the 1999 Izmit and Düzce, Turkey, earthquakes, N. Toksöz (Ed.).

Hollingsworth, J., Dolan, J.F., Milliner, C.W., Leprince, S., Ayoub, F., Avouac, J.-P., 2012. Analysis of the shallow slip deficit using sub-pixel image correlation: implications for fault slip rates, and seismic hazards. Eos Trans. AGU 93. Fall 2012 meeting, abstract T23H-02.

Humphreys, E.D., Weldon, R.J., 1994. Deformation across the western United States: A local estimate of Pacific–North America transform deformation. J. Geophys. Res. 99, 19975–20010.

Jachens, R.C., Langenheim, V.E., Matti, J.C., 2002. Relationship of the 1999 Hector Mine and 1992 Landers fault ruptures to offsets on Neogene faults and distribution of Late Cenozoic basins in the eastern California shear zone. Bull. Seismol. Soc. Am. 92, 1592–1605.

Jacobs, A., Sandwell, D., Fialko, Y., Sichoix, L., 2002. The 1999 (M_w 7.1) Hector Mine, California, earthquake: Near-field postseismic deformation from ERS interferometry. Bull. Seismol. Soc. Am. 92, 1433–1442.

Jónsson, S., Zebker, H., Segall, P., Amelung, F., 2002. Fault slip distribution of the 1999 M 7.1 Hector Mine, California earthquake, estimated from satellite radar and GPS measurements. Bull. Seismol. Soc. Am. 92 (4), 1377–1389.

Kaneko, Y., Fialko, Y., 2011. Shallow slip deficit due to large strike-slip earthquakes in dynamic rupture simulations with elasto-plastic off-fault response. Geophys. J. Int. 186, 1389–1403.

Kaneko, Y., Fialko, Y., Sandwell, D.T., Tong, X., Furuya, M., 2013. Interseismic deformation and creep along the central section of the North Anatolian fault (Turkey): InSAR observations and implications for rate-and-state friction properties. J. Geophys. Res. 118, 316–331. http://dx.doi.org/10.1029/2012JB009661.

Karabacak, V., Altunel, E., Çakir, Z., 2011. Monitoring aseismic surface creep along the North Anatolian fault (Turkey) using ground-based LIDAR. Earth Planet. Sci. Lett. 304, 64–70. http://dx.doi.org/10.1016/j.epsl.2011.01.017.

King, G.C.P., Wesnousky, S.G., 2007. Scaling of fault parameters for continental strike-slip earthquakes. Bull. Seismol. Soc. Am. 97, 1833–1840.

Kozaci, Ö., Dolan, J.F., Finkel, R.C., Hartleb, R.D., 2007. A 2000-year slip rate for the North Anatolian fault, Turkey, from cosmogenic 36Cl geochronology: Implications for the constancy of fault loading and slip rates. Geology 35, 867–870. http://dx.doi.org/10.1130/G23187A.1.

Kozaci, Ö., Dolan, J.F., Finkel, R.C., 2009. Late Holocene slip rate for the central North Anatolian fault, Tahtakorpru, Turkey, from cosmogenic ^{10}Be geochronology: Implications for the constancy of fault loading and strain release rates. J. Geophys. Res. 114. http://dx.doi.org/10.1029/2008JB005760.

Lasserre, C., Peltzer, G., Crampé, F., Klinger, Y., Van der Woerd, J., Tapponnier, P., 2005. Coseismic deformation of the 2001 $M_w = 7.8$ Kokoxili earthquake in Tibet, measured by synthetic aperture radar interferometry. J. Geophys. Res. 110, B12408. http://dx.doi.org/10.1029/2004JB003500.

Leprince, S., Barbot, S., Ayoub, F., Avouac, J.P., 2007. Automatic and precise orthorectification, coregistration, and subpixel correlation of satellite images, application to ground deformation measurements. IEEE Trans. Geosci. Remote Sens. 45 (6), 1529–1558.

Leprince, S., Berthier, E., Ayoub, F., Delacourt, C., Avouac, J.P., 2008. Monitoring earth surface dynamics with optical imagery. Eos Trans. AGU 89 (1), 1–2.

Li, Y.-G., Vidale, J.E., Aki, K., Marone, C., Lee, W.H.K., 1994. Fine structure of the Landers fault zone, segmentation and the rupture process. Science 265, 367–370.

Li, Y.-G., Vidale, J.E., Aki, K., Xu, F., Burdette, T., 1998. Evidence of shallow fault zone strengthening after the 1992 M7.5 Landers, California, earthquake. Science 279, 217–219.

Li, Y.-G., Aki, K., Vidale, J.E., Xu, F., 1999. Shallow structure of the Landers fault zone from explosion-generated trapped waves. J. Geophys. Res. 104, 20257–20275.

Li, Y.-G., Vidale, J.E., et al., 2004. Low-velocity damaged structure of the San Andreas Fault at Parkfield from fault zone trapped waves. Geophys. Res. Lett. 31.

Lienkaemper, J.J., McFarland, F.S., Simpson, R.W., Bilham, R.G., Ponce, D.A., Boatwright, J.J., Caskey, S.J., 2012. Long-term creep rates on the Hayward Fault: Evidence for controls on the size and frequency of large earthquakes. Bull. Seismol. Soc. Am. 102 (1), 31–41. http://dx.doi.org/10.1785/0120110033.

Lindsey, E.O., Fialko, Y., 2013. Geodetic slip rates in the southern San Andreas Fault system: Effects of elastic heterogeneity and fault geometry. J. Geophys. Res. 118, 689–697. http://dx.doi.org/10.1029/2012JB009358.

Lindsey, E.O., Sahakian, V., Fialko, Y., Bock, Y., Barbot, S., Rockwell, T., in press. Interseismic strain localization in the San Jacinto fault zone. Pure Appl. Geophys. http://dx.doix.org/10.1007/s00024-013-0753-z.

Liu, J., Sieh, K., Hauksson, E., 2003. A structural interpretation of the aftershock "Cloud" of the 1992 M_w 7.3 Landers earthquake. Bull. Seismol. Soc. Am. 93, 1333–1344.

Loveless, J.P., Meade, B.J., 2011. Partitioning of localized and diffuse deformation in the Tibetan Plateau from joint inversions of geologic and geodetic observations. Earth Planet. Sci. Lett. 303 (1–2), 11–24.

Lowey, G.W., 1998. A new estimate of the amount of displacement on the Denali fault system based on the occurrence of carbonate megaboulders in the Dezadeash Formation (Jura-Cretaceous), Yukon, and the Nutzotin Mountains sequence (Jura-Cretaceous), Alaska. Bull. Can. Pet. Geol. 46, 379–386.

Lozos, J.C., Oglesby, D.D., Brune, J.N., 2013. The effects of fault stepovers on ground motion. Bull. Seismol. Soc. Am. 103 (3), 1922–1934.

Ma, S., 2008. A physical model for widespread near-surface and fault zone damage induced by earthquakes. Geochem. Geophys. Geosyst. 9, Q11009. http://dx.doi.org/10.1029/2008GC002231.

Ma, S., Andrews, D.J., 2010. Inelastic off-fault response and three-dimensional dynamics of earthquake rupture on a strike-slip fault. J. Geophys. Res. 115, B04304. http://dx.doi.org/10.1029/2009JB006382.

Manighetti, I., King, G., Gaudemer, Y., Scholz, C., Doubre, C., 2001. Slip accumulation and lateral propagation of active normal faults in Afar. J. Geophys. Res. 106 (B7), 13667–13696.

Manighetti, I., King, G., Sammis, C.G., 2004. The role of off-fault damage in the evolution of normal faults. Earth Planet. Sci. Lett. 217, 399–408.

McGill, S.F., Wells, S.G., Fortner, S.K., Kuzma, H.A., McGill, J.D., 2009. Slip rate of the western Garlock fault, at Clark Wash, near Lone Tree Canyon, Mojave Desert, California. Geol. Soc. Am. Bull. 121, 536–554. http://dx.doi.org/10.1130/B26123.

Meade, B.J., Hager, B.H., 2005. Block models of crustal motion in southern California constrained by GPS measurements. J. Geophys. Res. 110, B03403. http://dx.doi.org/10.1029/2004JB003209. 19 pp.

Miller, M.L., Bradley, D.C., Bundtzen, T.K., McClelland, W.C., 2002. Late Cretaceous through Cenozoic strike-slip tectonics of Southwestern Alaska. J. Geol. 110, 247–270.

Milliner, C.W., Hollinsworth, J., Dolan, J.F., Leprince, S., Ayoub, F., Avouac, J.-P., 2012. Analysis of the shallow slip deficit using sub-pixel image correlation: examples from various large continental strike-slip earthquakes. Eos Trans. AGU 93. Fall 2012 meeting, abstract T13D-2652.

Nockleberg, W.J., Jones, D.L., Silberling, N.J., 1985. Origin and tectonic evolution of the Maclaren and Wrangellia terranes, eastern Alaska Range, Alaska. Geol. Soc. Am. Bull. 96, 1251–1270.

Oglesby, D.D., Mai, M., 2012. Fault geometry, rupture dynamics and ground motion from potential earthquakes on the North Anatolian Fault under the Sea of Marmara. Geophys. J. Int. 188, 1071–1087. http://dx.doi.org/10.1111/j.1365-246X.2011.05289.x.

Oskin, M., Iriondo, A., 2004. Large-magnitude transient strain accumulation on the Blackwater fault, Eastern California shear zone. Geology 32 (4), 313–316. http://dx.doi.org/10.1130/G20223.

Oskin, M., Perg, L., Shelef, E., Strane, M., Gurney, E., Singer, B., Zhang, X., 2008. Elevated shear zone loading rate during an earthquake cluster in eastern California. Geology 36 (6), 507–510.

Peltzer, G., Crampe, F., Hensley, S., Rosen, P., 2001. Transient strain accumulation and fault interaction in the Eastern California shear zone. Geology 29, 975–978.

Peng, Z., Ben-Zion, Y., Michael, A.J., Zhu, L., 2003. Quantitative analysis of fault zone waves in the rupture zone of the Landers, 1992, California earthquake: Evidence for a shallow trapping structure. Geophys. J. Int. 155, 1021–1041. http://dx.doi.org/10.1111/j.1365-246X.2003.02109.

Reed, B.L., Lanphere, M.A., 1974. Offset plutons and history of movement along the McKinley segment of the Denali Fault system, Alaska. Geol. Soc. Am. Bull. 85, 1883–1892.

Reilinger, R.E., Ergintav, S., Bürgmann, R., McClusky, S., Lenk, O., Barka, A., Gurkan, O., Hearn, L., Feigl, K.L., Cakmak, R., Aktug, B., Ozener, H., Töksoz, M.N., 2000. Coseismic and postseismic fault slip for the 17 August 1999, M = 7.5, Izmit, Turkey earthquake. Science 289, 1519–1524. http://dx.doi.org/10.1126/science.289.5484.1519.

Rockwell, T.K., Lindvall, S., Dawson, T., Langridge, R., Lettis, W., Klinger, Y., 2002. Lateral offsets on surveyed cultural features resulting from the 1999 Izmit and Duzce earthquakes, Turkey. Bull. Seismol. Soc. Am. 92 (1), 79–94.

Sammis, C.G., Rosakis, A.J., Bhat, H.S., 2009. Effects of off-fault damage on earthquake rupture propagation: experimental studies. Pure Appl. Geophys. 166, 1629–1648. http://dx.doi.org/10.1007/s00024-009-0512-3.

Sauber, J., Thatcher, W., Solomon, S.C., Lisowski, M., 1994. Geodetic slip rate for the eastern California shear zone and the recurrence time of Mojave Desert earthquakes. Nature 367, 264–266.

Savage, J.C., Burford, R.O., 1973. Geodetic determination of relative plate motion in central California. J. Geophys. Res. 78 (5), 832–845.

Savage, J.C., Lisowsky, M., Prescott, W.H., 1990. An apparent shear zone trending north northwest across the Mojave Desert into Owens Valley, eastern California. Geophys. Res. Lett. 12, 2113–2116.

Scholz, C.H., 2002. The Mechanics of Earthquakes and Faulting. Cambridge University Press.

Schulz, S.S., Mavko, G.M., Burford, R.O., Stuart, W.D., 1982. Long-term fault creep observations in central California. J. Geophys. Res. 87, 6977–6982. http://dx.doi.org/10.1029/JB087iB08p06977.

Segall, P., Pollard, D.D., 1983. Nucleation and growth of strike slip faults in granite. J. Geophys. Res. 88, 555–568. http://dx.doi.org/10.1029/JB088iB01p00555.

Sengör, A.M.C., 1979. The North Anatolian transform fault: Its age, offset and tectonic significance. J. Geol. Soc. 136, 269–282.

Shelef, E., Oskin, M., 2010. Deformation processes adjacent to active faults: Examples from eastern California. J. Geophys. Res. 115, B05308. http://dx.doi.org/10.1029/2009JB006289.

Sieh, K.E., 1978. Slip along the San Andreas fault associated with the great 1857 earthquake. Bull. Seismol. Soc. Am. 68, 1421–1448.

Simons, M., Fialko, Y., Rivera, L., 2002. Coseismic deformation from the 1999 M_w 7.1 Hector Mine, California, earthquake as inferred from InSAR and GPS observations. Bull. Seismol. Soc. Am. 92, 1390–1402.

Stirling, M.W., Wesnousky, S.G., Shimazaki, K., 1996. Fault trace complexity, cumulative slip, and the shape of the magnitude–frequency distribution for strike-slip faults: a global survey. Geophys. J. Int. 124, 833–868.

Sudhaus, H., Jónsson, S., 2011. Source model for the 1997 Zirkuh earthquake (M_W = 7.2) in Iran derived from JERS and ERS InSAR observations. Geophys. J. Int. 185 (2), 676–692.

Tchalenko, J.S., 1970. Similarities between shear zones of different magnitudes. Geol. Soc. Am. Bull. 81, 1625–1640.

Thatcher, W., Bonilla, M.G., 1989. Earthquake fault slip estimation from geologic, geodetic and seismologic observations: implications for earthquake mechanics and fault segmentation. USGS Open-File Report 89 (315). pp. 386–399.

Treiman, J., Kendrick, K.J., Bryant, W.A., Rockwell, T.K., McGill, S.F., 2002. Primary surface rupture associated with the M 7.1 16 October 1999 Hector Mine earthquake, San Bernardino County, California. Bull. Seismol. Soc. Am. 92 (4), 1171–1191.

Van Dissen, R., Barrell, D., Litchfield, N., King, A., Quigley, M., Villamor, P., Furlong, K., Mackenzie, H., Klahn, A., Begg, J., Townsend, D., Stahl, T., Noble, D., Duffy, B., Bilderback, E., Jongens, R., Cox, S., Langridge, R., Ries, W., Dhakal, R., Smith, A., Nicol, R., Pedley, K., Henham, H., Hunter, R., 2011. Surface rupture displacement on the Greendale fault during the M_w 7.1 Darfield (Canterbury) earthquake, New Zealand, and its impact on man-made structures. In: Proceedings Ninth Pacific Conference on Earthquake Engineering, Building an Earthquake-Resilient Society. Auckland, New Zealand, 14–16 April, 2011. New Zealand Society for Earthquake Engineering, Paper 186, 8 pp.

Vermilye, J., Scholz, C., 1998. The process zone: A microstructural view of fault growth. J. Geophys. Res. 103 (B6), 12223–12237.

Walker, R., Jackson, J., 2004. Active tectonics and late Cenozoic strain distribution in central and eastern Iran. Tectonics 23, TC5010. http://dx.doi.org/10.1029/2003TC001529.

Wesnousky, S.G., 1988. Seismological and structural evolution of strike-slip faults. Nature 335, 340–343.

Wright, T.J., Lu, Z., Wicks, C., 2004. Constraining the slip distribution and fault geometry of the M-w 7.9, 3 November 2002, Denali fault earthquake with interferometric synthetic aperture radar and global positioning system data. Bull. Seismol. Soc. Am. 94, S175–S189.

Xu, X., Yu, G., Klinger, Y., Tapponnier, P., Van der Woerd, J., 2006. Re-evaluation of surface rupture parameters and faulting segmentation of the 2001 Kunlunshan earthquake (M_w 7.8), northern Tibet plateau, China. J. Geophys. Res. 111, B05316. http://dx.doi.org/10.1029/2004JB003488.

Zhang, P., Burchfiel, B.C., Chen, S., Deng, Q., 1989. The extinction of pull-apart basins. Geology 17, 814–817.